Geochemical Journal, Vol. 50, pp. 477 to 492, 2016 doi:10.2343/geochemj.2.0428

3D characteristics of ADCP echo intensity anomaly observed over the Snail, Archean, and Pika hydrothermal vent fields in the South Mariana Trough

KANAE KOMAKI,[1]* YASUO FURUSHIMA[2] and HIROYUKI YAMAMOTO[2]

[1]Center for Advanced Marine Core Research, Kochi University, 200 Monobe-Otsu, Nankoku-shi, Kochi 783-8502, Japan
[2]Japan Agency for Marine-Earth Science and Technology (JAMSTEC),
2-15 Natsushima-cho, Yokosuka, Kanagawa 237-0061, Japan

(*Received January 30, 2015; Accepted June 6, 2016*)

We conducted four dives using the Urashima autonomous underwater vehicle (AUV) over three hydrothermal vent fields (Snail, Archean, and Pika) within the South Mariana Trough in July 2009, and measured the echo intensity (EI) with an acoustic Doppler current profiler (ADCP) mounted on the AUV. The ADCP data produced 3D structures of the EI over the vents, which clearly showed higher EI anomalies over the Pika and Archean vents. The characteristics of the higher EI anomalies were carefully examined and described in terms of their relationships with turbidity that was simultaneously observed with a single point turbidity sensor. It is plausible that the higher EI anomaly indicates the thickness of the plumes at some locations (i.e., 230 m thickness at the Pika site, 140 m at the Archean, and 160 m at the Snail) where both the turbidity and EI have a signal. The results also explain the long-term southwestward advection of the higher anomaly water by the local mean current.

Keywords: South Mariana Trough, hydrothermal plume, AUV, 3D mapping, ADCP echo intensity

INTRODUCTION

Hydrothermal plumes involving geochemical components are diffused and advected by thermal gradients and local currents or tides, with a great impact on the surrounding biological environments. Geochemical components become a source of the ambient microbial bloom in the plume, which results in a further bloom of the ambient zooplankton (Anderson *et al*., 2013). Thus, if we can obtain plume thickness and structure over a wide area, it would greatly improve analysis of the entire biomass distribution at the vent site (Yoshida-Takashima *et al*., 2012), as well as biomass interaction between hydrothermal water, cooler seawater, and the venting seafloor (Takai *et al*., 2001).

Historically, plume exploration has been conducted using water sampling and chemical single point sensors, which are accurate but not effective for mapping a large area at one time. Currently, by virtue of acoustic sensor technology, sound reflection against an object can be measured from various ranges, from which plume structure can be determined if the nature of the reflected objects is known. In a hydrothermal plume, Thomson *et al*. (1989, 1992) first analyzed the sound reflected by zooplankton by using plankton nets and acoustic observations from ADCPs during tow-yos over the Endeavour Ridge. They compared the ADCP sound beam and zooplankton density with regards to depth. Though the research focused on one dimension of depth, they effectively used acoustic technology to suggest the location and thickness of zooplankton in a plume.

More recent platform evolutions, such as sensors mounted on autonomous underwater vehicles (AUVs), have succeeded in measuring the lateral distribution of plumes, including vent sites (German *et al*., 2008; Baker *et al*., 2012). This has enabled us to determine and understand plume distribution in much more detail.

With this new platform technology, new features of hydrothermal plumes are being discovered by the application of acoustic sensors. Using side-scan sonars, the AUV "Urashima", owned by the Japan Agency for Marine-Earth Science and Technology (JAMSTEC), observed 100-m-high filaments and fog-like structures above the seabed in the Iheya-North Knoll (Kumagai *et al*., 2010) and the South Mariana Trough (Asada *et al*., 2011; Nakamura *et al*., 2013), which were interpreted as hydrothermal plumes just spouted out from vents. In repeat observations using cameras mounted on the ROPOS remotely operated vehicle (ROV) and the Shinkai 6500

*Corresponding author (e-mail: kana.komaki@yahoo.com)
*Present address (Aug. 2016~): School of Marine and Environmental Affairs, College of the Environment, University of Washington, 3707 Brooklyn Avenue NE, Seattle, WA 98105, U.S.A.

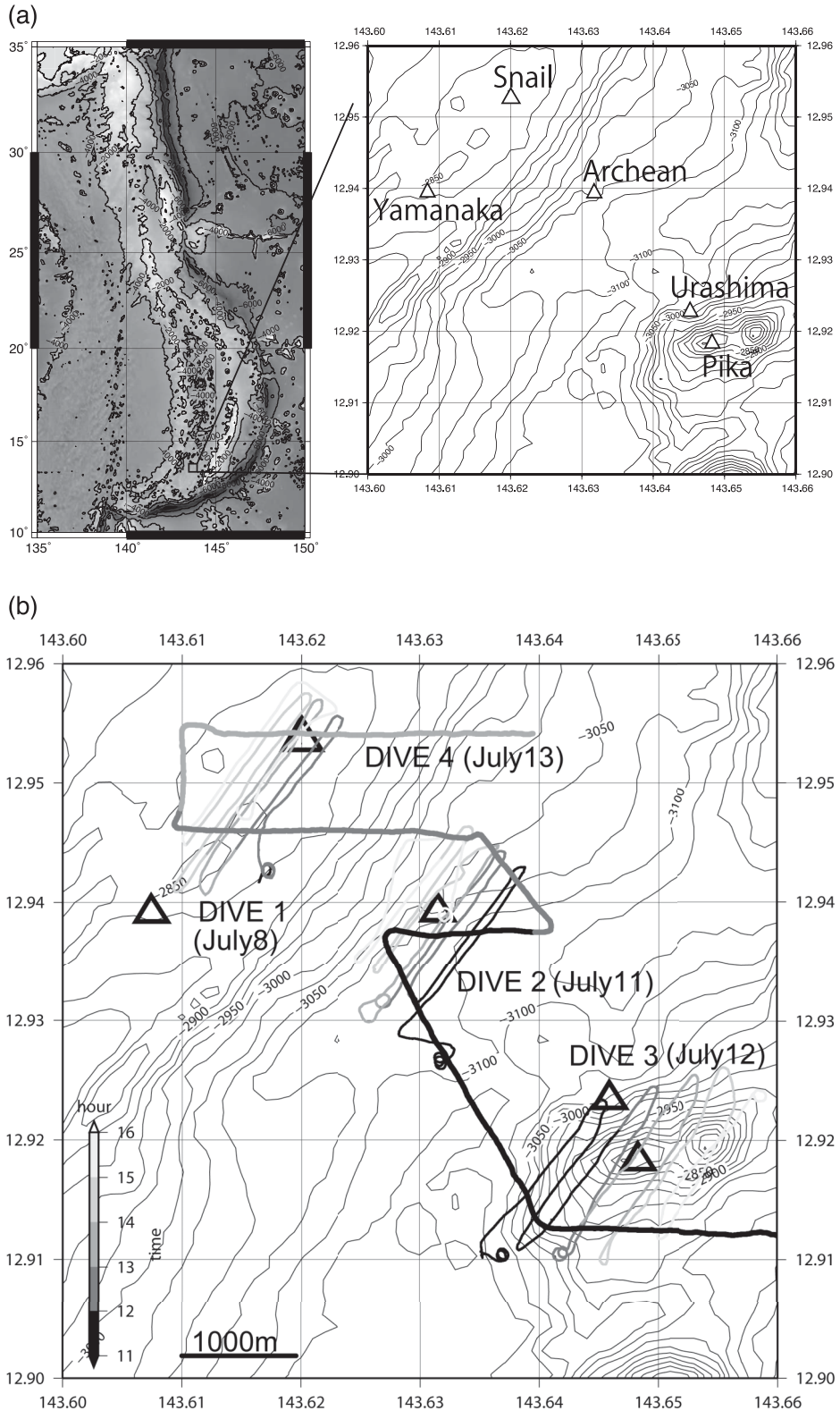

Fig. 1. (a) Topographic map of the observation area in the South Mariana Trough. In the enlarged map, solid contours show 25-m depth intervals, and triangles show the Snail, Archean and Pika sites (InterRidge Vents Database 2.2, 2015), the Yamanaka (Asada et al., 2015), and the Urashima site (Nakamura et al., 2013). (b) Track lines of the AUV dives. Dives 1, 2, and 3 were conducted over the Snail, Archean and Pika sites, respectively, at a 100-m altitude. Dive 4 was over the three sites at a 150-m altitude. Shadows indicate time [o'clock]. Triangles indicate the locations of the vents.

manned operated vehicle, Nakamura *et al*. (2013) confirmed a new vent to the north of the well-known Pika site, which was named the Urashima site. Using an acoustic Doppler current profiler (ADCP), Komaki *et al*. (2009, 2010) observed a patchy but high echo intensity (EI) 100 m above the seabed within the Izena Cauldron, Okinawa Trough. These high anomalies corresponded to turbidity maxima. A combination of acoustic sensors and AUVs/ROVs will certainly prove effective in the near future for obtaining the 3D structure of hydrothermal plumes, which will help us analyze the diffusive and advective features of water in hydrothermal areas.

In this paper, considering the importance of plume image capture, we present 3D images of EI maxima obtained by an ADCP mounted on the AUV, and describe, in detail, how the EI maxima correspond to hydrothermal plumes over the Snail, Archean, and Pika sites within the South Mariana Trough, where 3D plume imaging has never before been conducted. Earlier studies used echo from side-scanning sonars only for plume imaging; however, we quantitatively describe and compare the strength of the echo from the ADCP, and also discuss the effectiveness of the ADCP for future plume surveys.

Observations and Data Processing Method

The Snail site, also known as Fryer site, exists at a depth of 2880 m, at 12.9533°N and 143.6200°E on a spreading ridge (Wheat *et al*., 2003) in the South Mariana Trough (Fig. 1a). Baker *et al*. (2005) reported a large-scale extension of plumes from the Snail site along the ridge, observed by tow-yos of chemical sensors measuring turbidity and reduction-oxidation potential (Eh), the latter of which measures the ratio at which seawater is oxidized. Southwest of the Snail site, Yamanaka site is located at a depth of 2830 m, at 12.9403°N and 143.6080°E (Kakegawa *et al*., 2008; Asada *et al*., 2015). The Archean site is located at a depth of 2990 m, at 12.9400°N and 143.6317°E, southeast of the Snail site over a deep valley (JAMSTEC, 2009; InterRidge Vents Database 2.2, 2015). The Pika site is located at 2830 m depth, at 12.9183°N and 143.6483°E, on the top of mounds to the far southeast of the Archean site (Ishibashi *et al*., 2004).

During the R/V Yokosuka cruise of July 2009, known as the YK09-8 cruise (JAMSTEC, 2009), we conducted four dives of the Urashima AUV on July 8th, 11th, 12th, and 13th, over the three hydrothermal vent fields (Fig. 1b). Though the number of total dives of this AUV increased from 91 to 94 during the operations, the 91st dive was the first time that the Urashima had surveyed a hydrothermal area. The AUV was kept 100 m above the seabed over each of the Snail, Archean, and Pika sites (hereafter, Dives 1–3), but 150 m above the seabed when diving above all three mounds (hereafter, Dive 4).

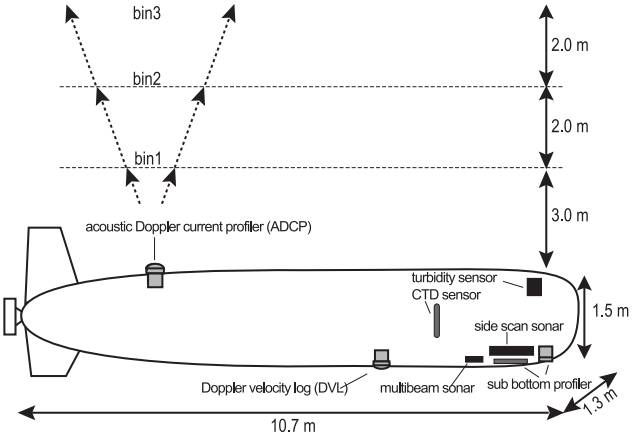

Fig. 2. Schematic of instruments and the AUV Urashima.

Specifications and equipment installed within the AUV payload (Fig. 2) are listed in Table 1. Since the present study aims to examine the extent and thickness of hydrothermal plumes, data from a conductivity-temperature-depth (CTD) sensor and a turbidity sensor were used.

In addition to such general, single-point chemical property sensor data, we used the ADCP EI data to estimate plume structure. The EI is the strength of a returning sound pulse that is reflected by scatterers in the water. A 600 kHz ADCP was mounted on the AUV, facing upward on the tail part (Fig. 2). This observed the EI of reflected sound pulses from 23 layers above the AUV every 3 seconds. The first layer (bin) was set at 3 m above the AUV and the last bin was 47 m above the AUV, with 2 m depth intervals in between.

Due to absorption in water, the raw EI value is usually attenuated by increasing the bins from the ADCP transducers (Figs. 3a and 3c). Therefore, we removed the attenuation effect from the raw EI using the following procedure from Komaki *et al*. (2009). Firstly, all EI profiles were averaged in each bin to produce a mean EI profile (Fig. 3c). Secondly, the difference between the mean EI profile and each EI profile was calculated for each bin, producing an EI anomaly profile (Fig. 3d). This process removes the attenuation effect easily and effectively (Fig. 3b). Lastly, the EI anomaly profiles were averaged temporally every 20 seconds (approximately 10 m horizontally), and vertically at 10 m depths.

Results

3D distribution of the EI anomaly

3D distributions of EI anomalies in the Pika, Archean, and Snail sites and for Dive 4 (over all sites) are shown in Figs. 4a and 4b, respectively. In the figures, one cube

Table 1. Specifications and equipment of the AUV Urashima

AUV		
Specifications	Maximum operation depth	3500 m
	Maximum cruising distance	130 km
	Speed	0–2.7 knot
	Length	10 m
	Width	1.3 m
	Height	1.5 m
	Weight in the air	6.5 tonnes
	Power system	Rechargeable Li ion cell
AUV equipments		
Multibean sonar	Product name	SeaBat 7125
	Frequency	400 kHz
	Sector coverage	128 deg
	Number of beams	256
	Resolution	6 mm
Side scan sonar	Product name	Edgtech 2200M
	Frequency	120 kHz (chirp)
	Range	300 m
Subbottom profiler	Product name	Edgtech 2200M
	Frequency	1–6 kHz (chirp)
	Resolution	15–25 cm
ADCP	Product name	Workhorse ADCP
	Frequency	600 kHz
CTD	Product name	SBE19+
	Sensors	temperature, conductivity, depth, oxygen
Turbidity sensor	Product name	ATU6-CMP
	Resolution	0.0002 FTU

represents 10 m in height and 20 seconds in time, and the color indicates the averaged EI anomaly in the cube, as described in the previous section. Thick layers of EI anomalies higher than 0.8 counts are found at the top of the mound of the Pika site (Fig. 4a) and over the valley of the Archean (Figs. 4a and 4b). In the Snail site, the anomaly is lower and more dispersed (Fig. 4a).

Turbidity-EI anomaly relationships

The horizontal distributions of turbidity in the Pika, Archean, Snail, and Dive 4 sites are shown in Figs. 5a and 5b, which were obtained at the AUV depth and averaged every 20 seconds. Turbidity maxima stronger than 800 mV, which correspond to approximately 4 FTU, exist above the Pika and Archean, and slightly weaker maxima (790~800 mV) are dispersed above the Snail. No strong maxima were found in the Urashima and Yamanaka sites in this study.

The EI anomaly obtained in the ADCP first bin, which is the layer 3–5 m above the AUV, was measured in the water closest to the turbidity sensor. Therefore, the two properties were compared at each site to describe the EI anomaly characteristics. The EI anomaly used here was also averaged every 20 seconds.

Pika site (Dive 3) The turbidity variations have a much higher frequency and the maxima do not initially appear to match the EI anomaly maxima (Figs. 6a and 6b). However, we then used 300 second running means in order to compare the maxima on a larger scale. Strong turbidity maxima (defined here as greater than 775 mV) were found at 5 time periods centered at 11:15, 11:30, 11:55, 12:30, and 13:20 (T1–T5; Fig. 6a). The strongest maxima (T3, T4, and T5) exist just above the Pika site (Fig. 5a), indicating hydrothermal signals. Strong EI maxima (defined here as greater than 1 count) were found at 6 time periods centered at 10:40, 11:15, 11:35, 11:55, 12:25, and 13:20 (L1–L6; Fig. 6b). The turbidity maxima of T3, T4, and T5 are then contained within the EI maxima of L4, L5, and L6. The weak turbidity maximum (T1) coincides with the weak EI maximum (L2), and L1 coincides with a slight change in shape of the turbidity signal. The T2 value is unique; the raw turbidity value is momentarily quite high and nearly 900 mV, but the EI anomaly is continuously high.

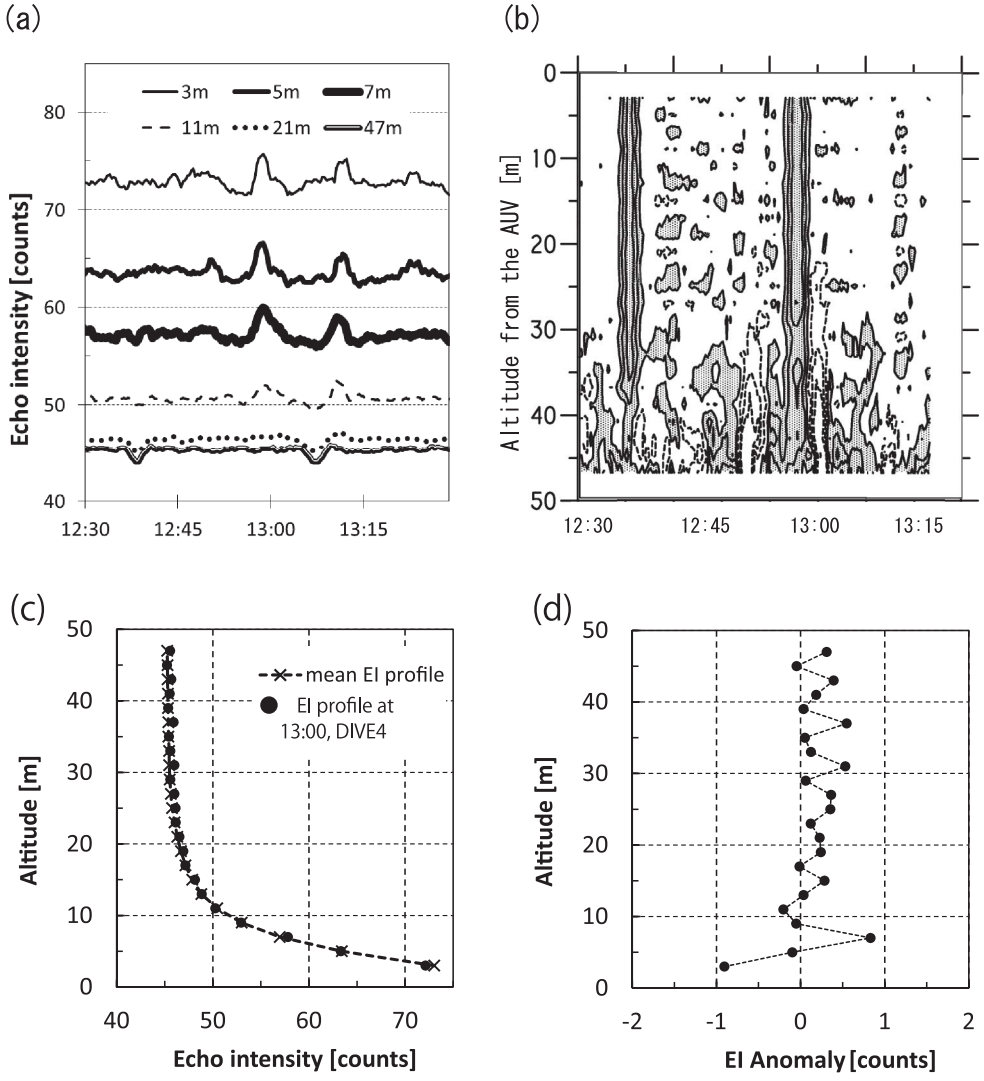

Fig. 3. (a) Temporal variations of raw echo intensity [counts] at depths of 3 m, 5 m, 11 m, 21 m, 31 m, and 41 m above the AUV between 12:30–13:30 in Dive 4. (b) A vertical section of echo intensity anomaly [counts] with regards of altitudes [m] above the AUV between 12:30–13:30 in Dive 4. Shades show negative anomaly area. (c) The mean EI profile from all dives data at depths greater than 2600 m, and a snap-shot EI profile, with altitudes [m] above the AUV. (d) The EI anomaly profile at 13:00 of Dive 4 subtracted the EI profiles described in (c).

Archean site (Dive 2) Turbidity maxima were compared to EI anomaly maxima at the Archean site. 10 strong turbidity maxima (>775 mV) were found at 10:45, 11:05, 12:45, 13:05, 13:35, 14:15, 15:15, 15:40, and 15:55 (T1–T10; Fig. 6c). The T5, T6, T7, T8, and T9 maxima are close to the vent, which indicates a hydrothermal plume signal. Strong EI maxima (>1 count) exist only in the latter half of the dive at 13:35, 14:15, 14:35, 15:05, and 16:00 (L1–L5; Fig. 6d). The T5, T6, T7, and T10 maxima correspond to those of L1, L2, L3, and L5, however, the most prominent turbidity maxima, T9, does not coincide with an EI anomaly.

Snail site (Dive 1) The turbidity at the Snail site is rather lower than that at the Pika and Archean sites, and there is no maximum stronger than 820 mV. Weak maxima (>775 mV) exist at 13:50, 14:25, 14:45, 15:00, 15:20, and 15:40 (T1–T6; Fig. 6e). As well as weak turbidity, there is no EI maximum exceeding 1 count (Fig. 6f). The turbidity maxima are mostly located above the Snail vent and away from the Yamanaka vent, except for T4 (Fig. 5a).

Over all sites (Dive 4) Similar to the Snail site, turbidity in Dive 4 is lower and there is no maximum stronger than 830 mV (Fig. 6g). Relatively weaker strong maxima (>775 mV) exist at 10:50, 11:00, 11:15, 11:25, 11:35, 11:50,

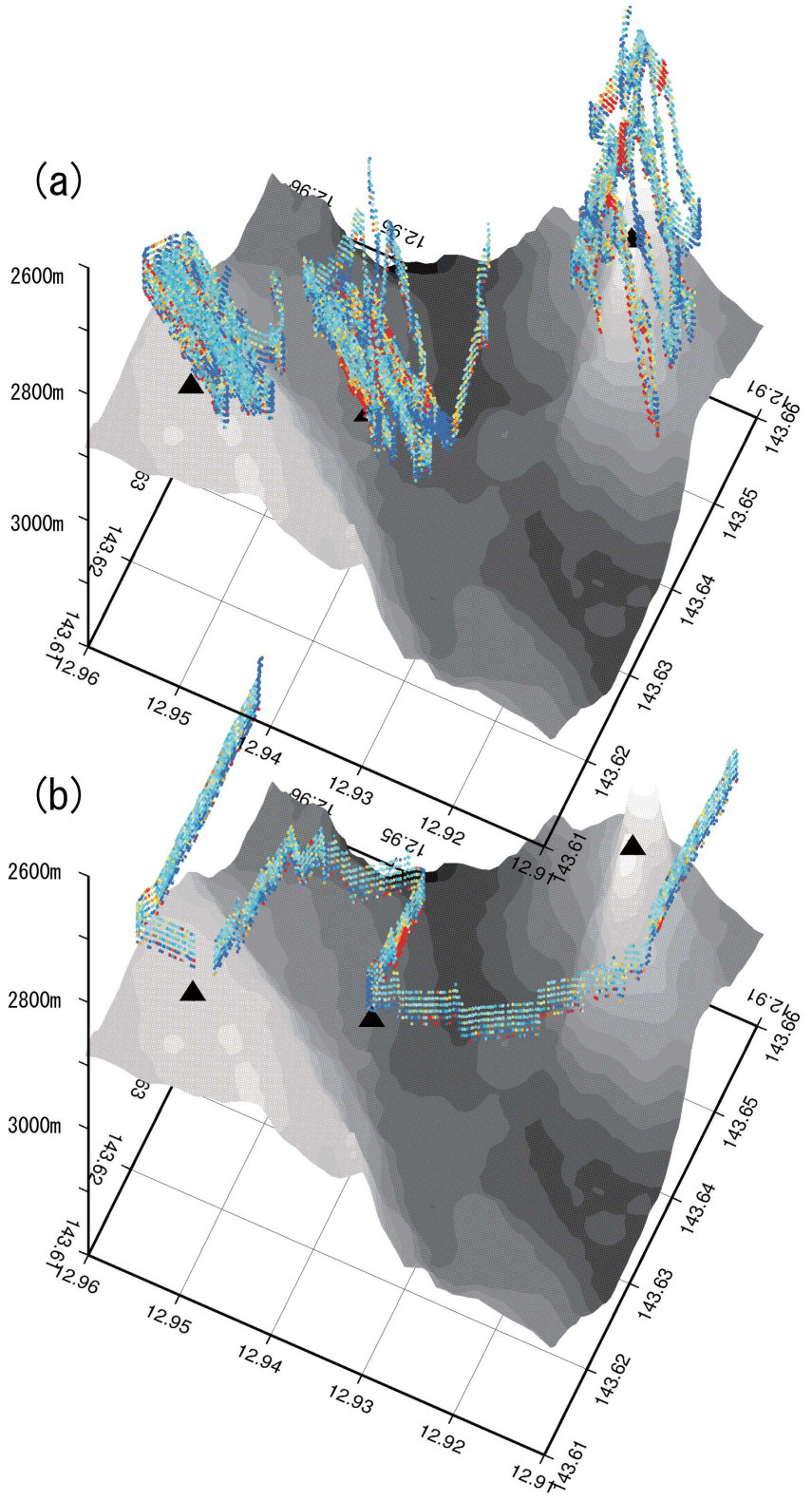

Fig. 4. 3D distributions of echo intensity anomaly for (a) Dives 1, 2, 3, and (b) Dive 4, from the view of 245 degrees azimuth with 70 degrees altitude. Each cube reflects an averaged value of 10 m in height and of 20 seconds in observation time. Color shows the intensity of the anomaly. Triangles represent the locations of the vents.

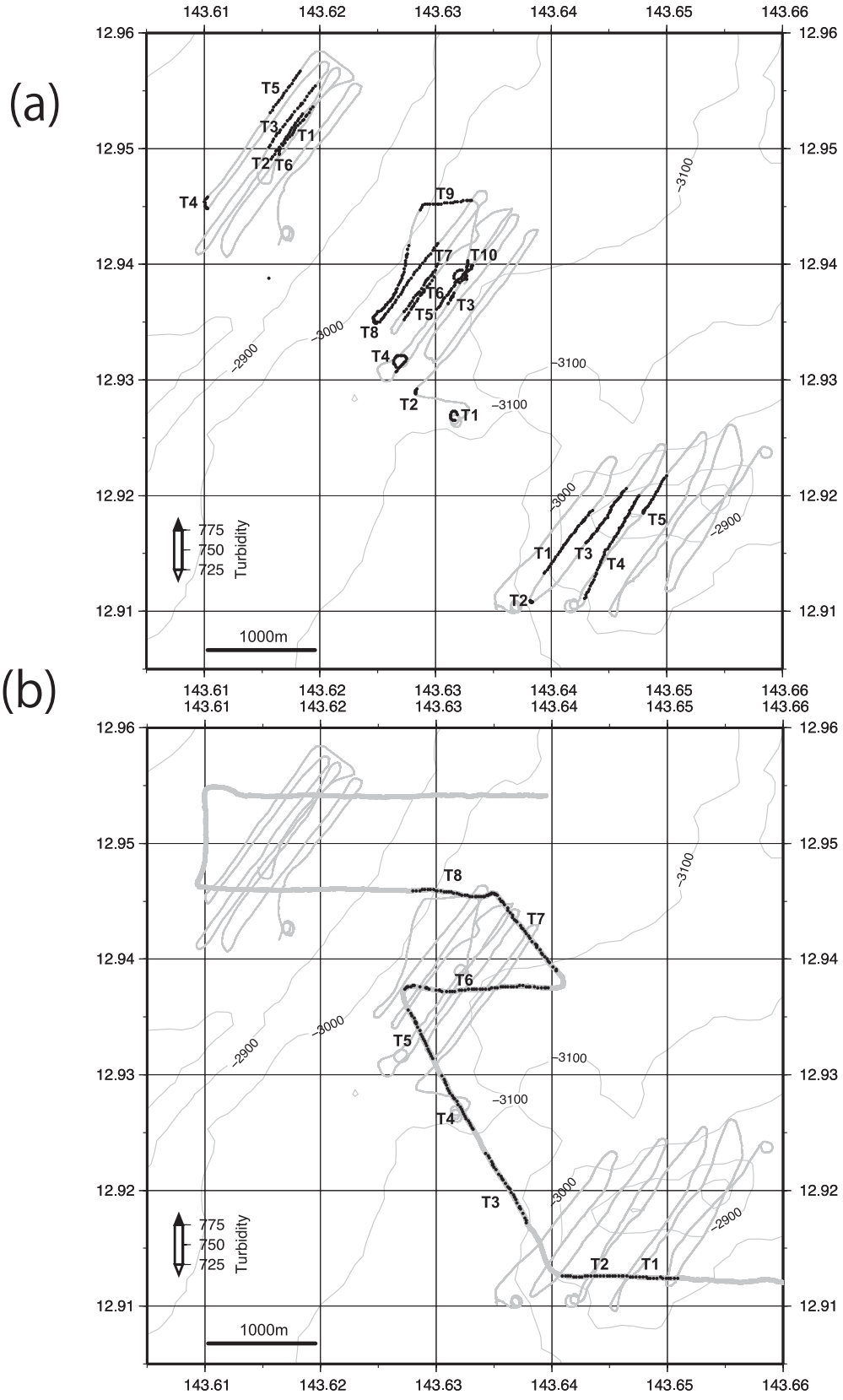

Fig. 5. Horizontal distributions of 300 seconds running means of turbidity [mV] at the AUV depth in Dives 1–3 (a), and in Dive 4 (b). Triangles indicate the locations of the vents.

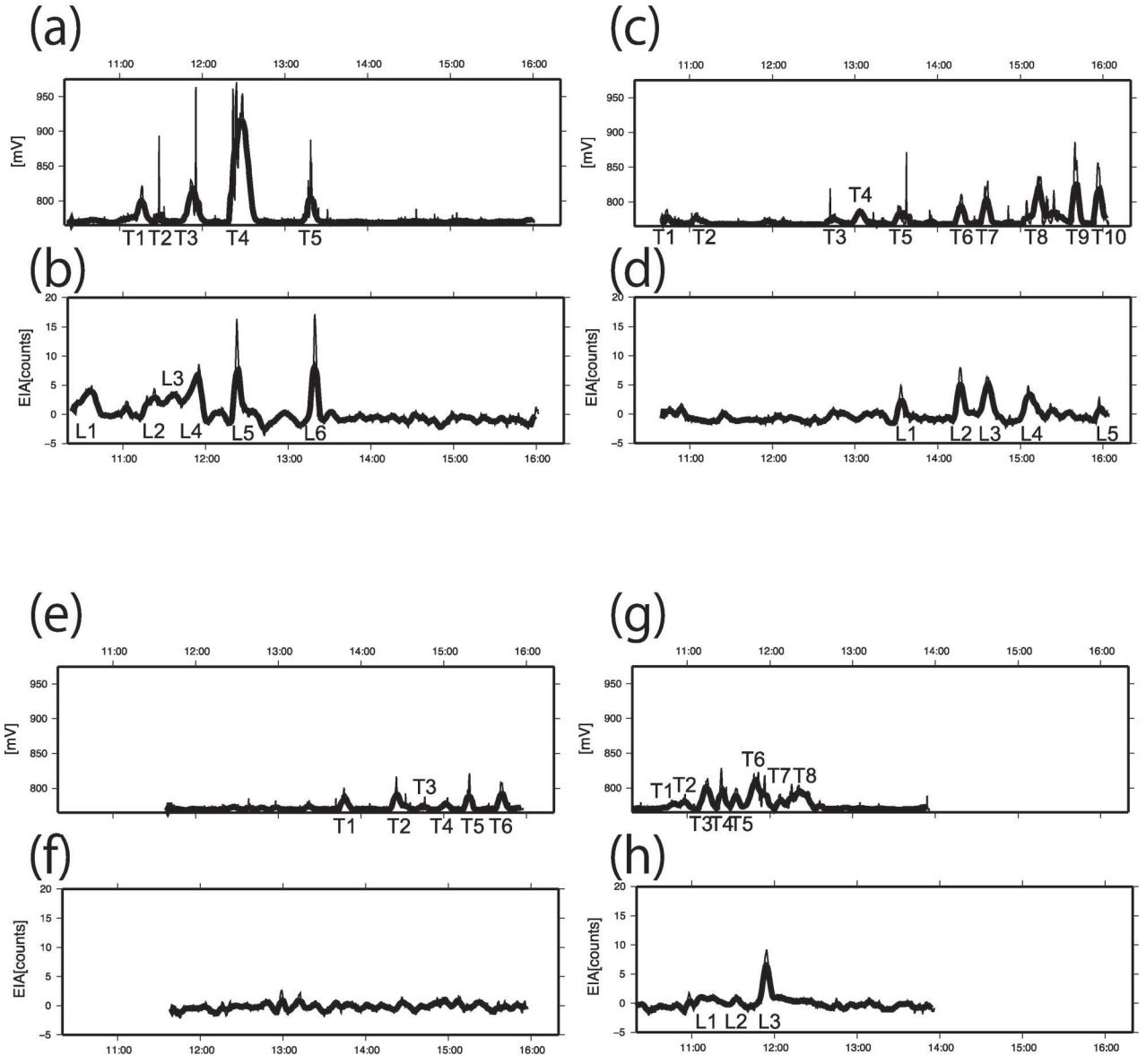

Fig. 6. Temporal variations of turbidity [mV; upper panel] and echo intensity anomaly [counts; lower panel] in Dive 3 over the Pika (a, b), Dive 2 over the Archean (c, d), Dive 1 over the Snail (e, f), and Dive 4 over all sites (g, h). Thin and thick lines represent the original values averaged every 20 seconds, and 300 seconds running means, respectively.

12:05, and 12:20 (T1–T8; Fig. 6g), and the maxima of T4–T8 are within the Archean. As for the EI anomaly, only three maxima are strong (>1 count) at 11:10, 11:35, and 11:55 (L1–L3; Fig. 6h). The strongest EI maximum of L3 coincides with the turbidity maximum of T6, which occurs near the Archean vent (Fig. 5b).

To summarize the relationships between turbidity and EI maxima, we conclude that they do not always correspond to each other. The maxima tend to coincide when both the turbidity and EI anomaly are sufficiently high close to the vents, such as T4 in the Pika and T6 in the Archean. However, even in the Archean, the most prominent turbidity maximum, T9, which is nearest the vent, does not correspond to the EI anomaly maximum.

This may be partly caused by a difference in measurement depth and mass between the two instruments. The turbidity sensor cannot detect a plume above the AUV, but the upward-looking ADCP can. Furthermore, turbidity can be more spatially and temporally variable than EI, because the turbidity sensor measures a point close to

the sensor whereas EI is the averaged value reflected from a far larger 2 m thick water mass. This discordance is discussed further in the following sections.

Characteristics of echo intensity anomaly over the vents

The EI anomaly data form a section; therefore, we describe the characteristics of the EI anomaly in terms of EI maxima distribution.

Pika site (Dive 3) A time series of the EI anomaly in the Pika shows that EI maximum layers exist over the top or middle of the western mound (Fig. 7a). The strong EI maximum layers (defined here as >0.5 counts) are approximately 40–60 m thick at depths of 2600–2750 m during the time periods centered at 11:55, 12:20, and 13:20 (C1–C3; Fig. 7a). These three EI maximum layers correspond well to the 1st bin EI maxima (L4–L6; Fig. 6b) described in the earlier section. If the EI maximum layer reflects a hydrothermal plume signal on the western mound of the Pika vent (2830 m), C1–C3 indicate that the thickness of this plume reaches approximately 230 m just above the vent.

The maximum layers exist over the eastern mound at around 12.922°N and 143.654°E, as well as over the western mound. They are also approximately 60 m thick during the time periods centered at 14:45 and 15:10 (C4, C5; Fig. 7a), and both the 1st bin EI anomaly and turbidity were not high at these locations (Figs. 6a and 6b).

At depths greater than the Pika vent, the high EI anomaly still exists along the mound slope, including the southwest side with a thickness of 10–20 m at depths of 2750–2940 m between 11:20–11:55, 2800–2850 m at 11:05, and 2850–2950 m between 10:40–10:50 (C′1–C′3; Fig. 7a). On the slope, the EI anomaly is stable and high at nearly 5 counts, however, only two maxima of turbidity (T1 and T2) were found, although the raw value of T2 is fairly high (895 mV; Fig. 6a).

The density of these EI maximum layers is much larger than those above the vent and the eastern mound (not shown), indicating that EI maxima characteristics differ between water that is shallower or deeper than the Pika vent. Thus, maps of the EI maxima core distribution were summarized for the upper/lower depths in order to describe the characteristics more clearly (Figs. 8a and 8b). At depths shallower than the Pika vent (<2830 m), most of the EI maxima are distributed in the western part of the mound, west of the Pika vent and south of the Urashima vent. Most strong EI cores, including the large C4 and C5 cores (core numbers are shown in Figs. 7 and 8), are located over the eastern mound, as described earlier. No maximum is found over the Urashima vent (12.922°N, 143.648°E, and 2922 m depth).

On the other hand, in layers deeper than the Pika vent, EI maximum cores such as C′1 and C′3 exist on the southwestern slope of the western mound at water depths of 2950–3100 m (Fig. 8b), where turbidity was briefly high at T2 (Fig. 6a). A few small cores, including C′2 and C′4, are close to the Urashima vent.

Archean site (Dive 2) In the Archean site, the maximum EI anomaly layer (>0.5 counts), 20–100 m thick, exists at depths of 2850–2960 m, not only over the 1st bin EI maxima of L1–L4 but also over areas of no turbidity or EI anomaly signal (Fig. 7b). For example, EI cores of C1 (core numbers are defined in Fig. 7b) between 11:25–11:30, C2 between 11:50–11:55, and C3 between 12:15–12:20 extend down from the top of the layer. In contrast to the latter four EI cores of C4–C7, the first three cores are located in the top of the layer as the AUV altitude becomes higher, though the core depth itself does not change. Thus, it is suggested that the sensors at the AUV depth did not capture the signal, as suggested in the previous section.

Most EI maximum cores are distributed in the southwest of the Archean vent, and core C4 is closest to the vent (Fig. 8c). The thickness of the hydrothermal plume from the Archean vent (2990 m) is expected to reach 140 m if these EI maximum cores indeed reflect a plume. Another higher EI anomaly layer is also shown at 2750–2800 m depth over the Archean vent between 12:50–12:55 (Fig. 7b), which is above the Snail vent depth of 2880 m.

Snail site (Dive 1) The higher EI anomaly at the Snail site is more dispersed and has a shorter duration compared to the other sections (Fig. 7c). As a whole, EI maximum cores exist in the lowermost or uppermost layers of the section (~2750 m and ~2700 m, respectively). As an example from the lowermost layer, core C1 between 12:20–12:30 is approximately 10–20 m thick and located at the east of the vent (Figs. 7c and 8d). This EI maximum core does not coincide with the turbidity maximum and the 1st EI maximum. The uppermost layer contains core C7 between 15:15–15:25, approximately 10–20 m thick, which is located at the west of the vent (Figs. 7c and 8d). This coincides with the turbidity maximum T5 (Fig. 6) and is close to the Snail vent. The potential density at the AUV depth also differs between each side of the vent; on the east side it is $27.729 < \sigma_\theta < 27.732$, but on the west side it is $27.731 < \sigma_\theta < 27.734$ (not shown). This result suggests that the water mass in this layer becomes elevated as it moves westward.

The map of EI maximum cores in Fig. 8d describes that most cores are distributed southwest of the Snail vent. If an EI maximum reflects a plume signal, the EI anomaly thickness in the eastern area is 160 m, as inferred from the vent depth (2880 m).

Over all sites (Dive 4) The EI maximum layer in Dive 4 is approximately 40 m thick at 2890–2930 m depth, and is situated at 12.936°N and 143.632°–143.400°E in the deep valley between the Pika and Archean sites (Figs. 7d and 8b). In this valley, several turbidity maxima exist

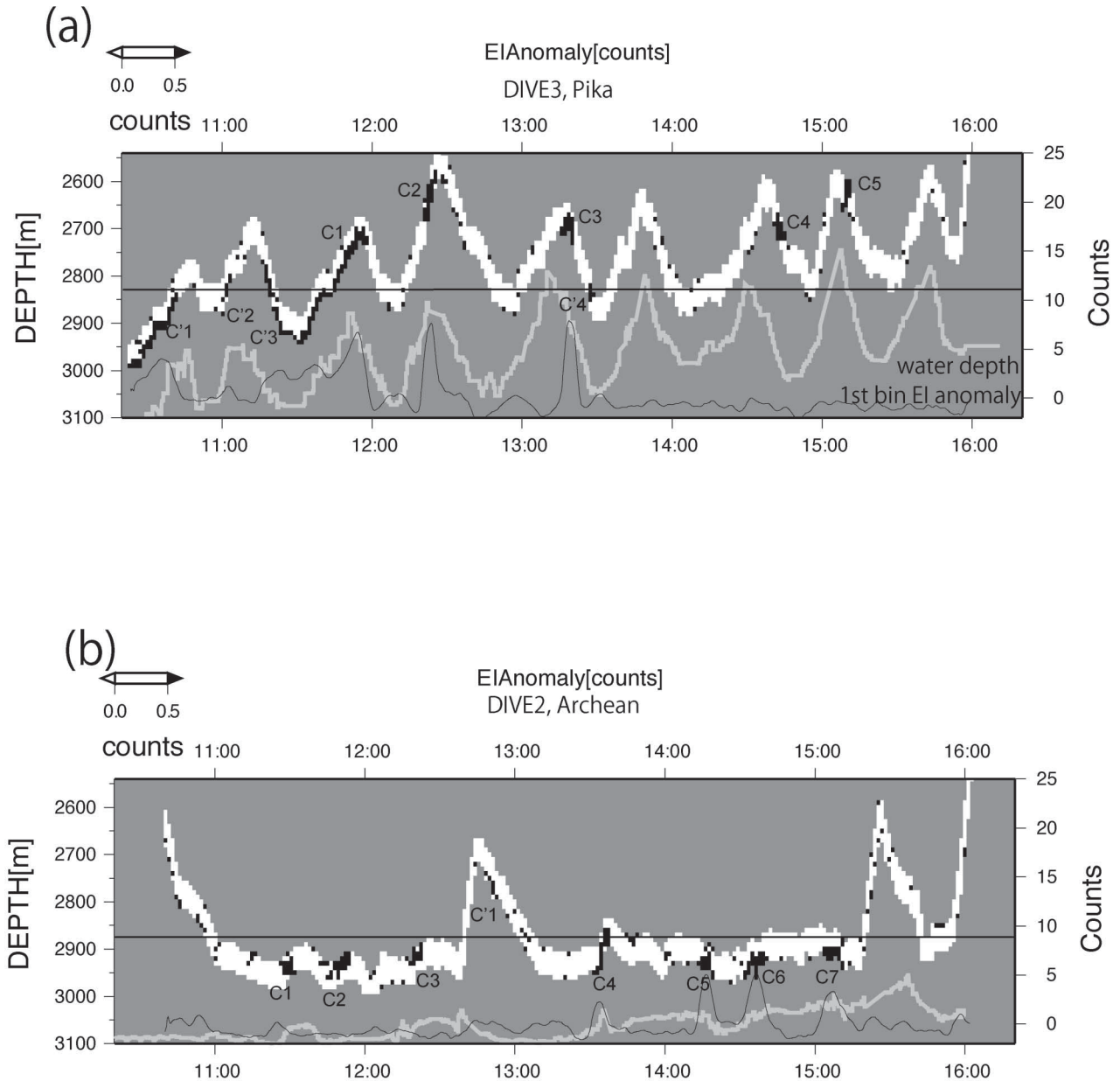

Fig. 7. Vertical sections of echo intensity anomaly [counts] with regards of diving time for (a) Dive 3 over the Pika, (b) Dive 2 over the Archean, (c) Dive 1 over the Snail, and (d) Dive 4 over all sites. Thick gray lines show water depth [m], and thin black line show the 1st bin echo intensity anomaly [counts]. The anomaly used here is averaged every 10 m grid in height and every 100 seconds in observation time, and the value stronger than 0.5 [counts] is only displayed.

(between 780–830 mV), and the depths are comparable to that of the Archean vent.

Plume distribution and advection

After a plume loses buoyancy, the plume exists in the same density layer assuming there is no local vertical circulation. Therefore, if the EI maxima are plume signals, the results suggest that the plume from the Pika vent is advected southwestward but some are advected eastward toward the eastern mound at shallower depths of the vent (Fig. 8a). The result showing low turbidity on the eastern mound is quite reasonable if the plume is only advected above the turbidity sensor depth. At greater depths, it is not plausible that the EI maxima on the western mound slope come from the Pika vent since the depth is too great (Fig. 8b). It is more reasonable if they originate from the

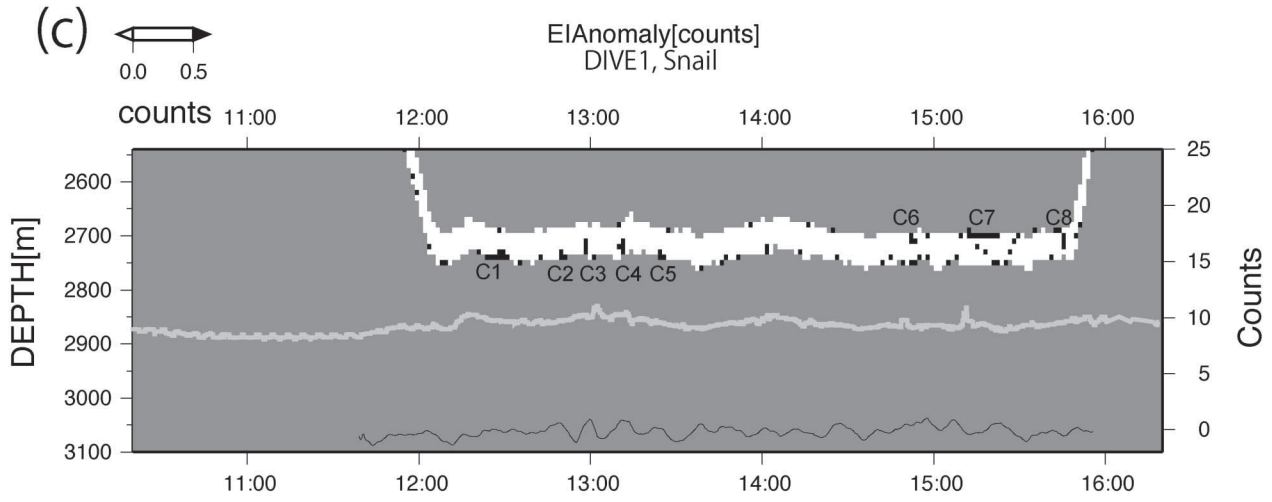

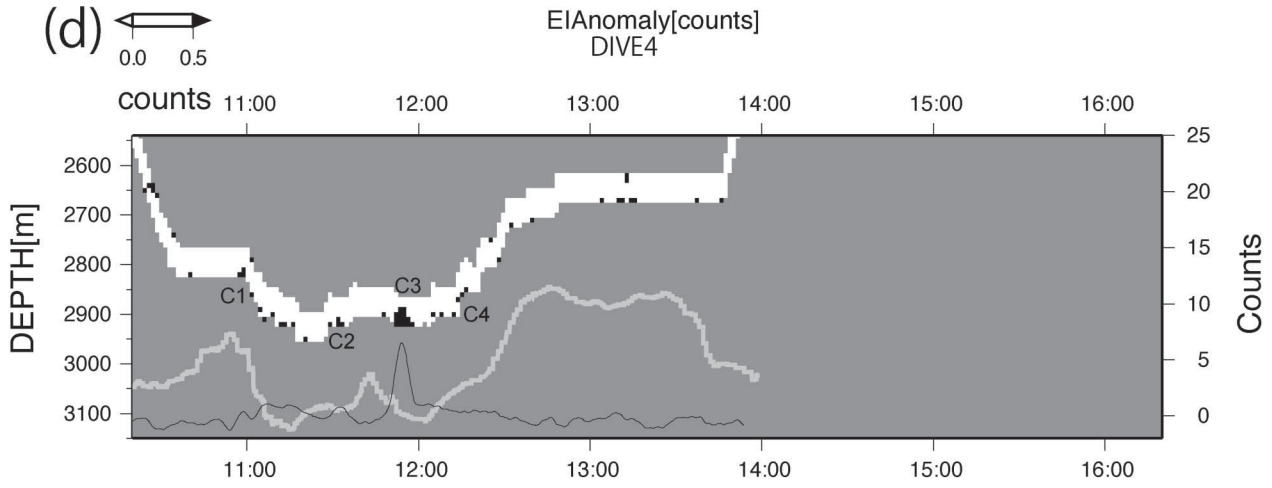

Fig. 7. (continued).

deeper Urashima vent (2922 m) or the Archean vent. Southwestward advection is consistent with the earlier plume study of Baker *et al*. (2005) and the moored current-meter results of Beaulieu *et al*. (2011). Nakamura *et al*. (2013) discovered a plume-like image above the Urashima vent from side-scanning sonar using the same cruise data as this study. As the image was captured at lower depths than the AUV depth, it is considered that the turbidity sensor and ADCP did not accurately detect the plume signal in this study.

Similar to the Pika site, the EI maximum cores from the Archean site might also be advected southwestward from the vent (Fig. 8c). The observation of some cores in the valley between the Archean and Pika sites by Dive 4 (C4, C5; Fig. 8c) indicates that plumes are advected southward and eastward from the vents. The turbidity sensor, which was just above the Archean vent, might not have detected the signal because the sensor might have been below the plume advection depth. By this assumption, the result suggests a remarkable ability of the ADCP to obtain data at multiple layers.

At the Snail site, it is expected that EI maxima are

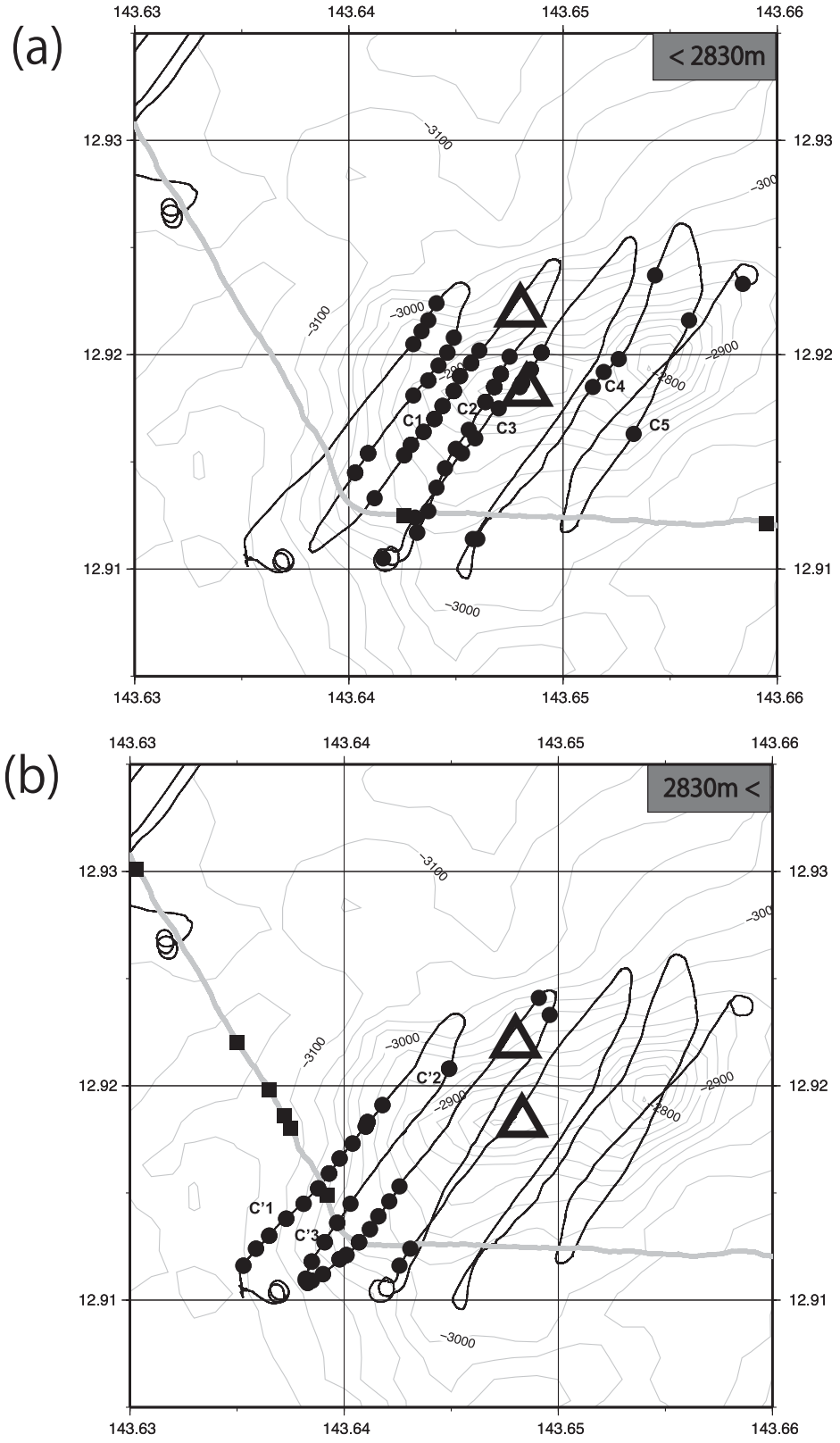

Fig. 8. Horizontal distributions of echo intensity anomaly higher than 0.5 [counts; circles and squares] and the core numbers suggested in Fig. 7 over the Pika at depths shallower than the Pika's vent depth (2830 m) (a), over the Pika at depths greater than 2830 m (b), over the Archean at depths greater than the Snail's vent depth (2880 m) (c), and over the Snail (d). Circles and squares represent the cores observed in Dives 1–3, and Dive 4, respectively. Triangles indicate the locations of the vents.

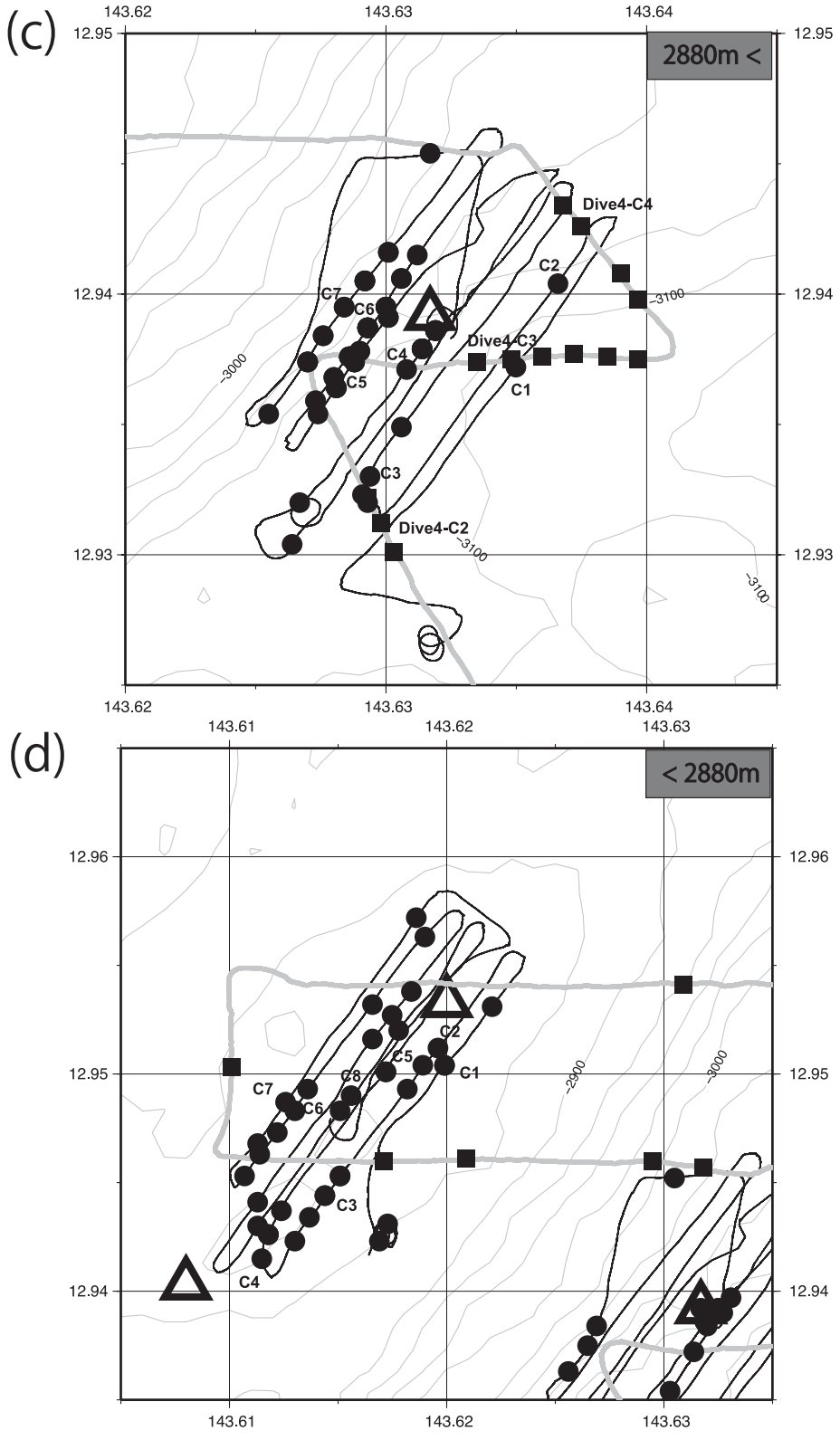

Fig. 8. (continued).

Table 2. Analysis patterns for turbidity and echo intensity anomaly from an upward-looking ADCP on the AUV for detecting hydrothermal plumes

Case	Signals		Most possible plume depths →	Analysis →	Next observation
	Turbidity	1st bin EI anomaly	X		
1	Y	Y	X ≤ AUV depth AUV depth ≤ X	· Examine EI anomaly maximum cores to confirm plume thickness in upper layer	· Down-looking ADCP to measure plume thickness in lower layer
2	Y	N	AUV depth ≤ X	· Confirm no plume signal by EI anomaly in upper layer	· Down-looking ADCP to measure plume thickness in lower layer
3	N	Y	X < AUV depth	· Examine EI anomaly maximum cores to confirm plume thickness in upper layer	· Confirm no plume signal by side-scanning sonar image in lower layer
4	N	N		· Confirm no plume signal by EI anomaly in upper layer	· Confirm no plume signal by side-scanning sonar image in lower layer

advected southwestward. Despite this, the core depth in the lowermost layer of the eastern sections becomes shallower towards the west. The density result supports this elevation data. Such a depth difference between water property isopleths east and west of the vent was also seen in the vertical section of the high turbidity anomalies on the T03A-02 line in Baker *et al*. (2005) (see their figure 5). It is expected that the turbidity sensor did not effectively detect the plume lower rim in the west, which is located far above the AUV.

In addition, the figure of Baker *et al*. (2005) shows a mirror image of the "C" shape of the plume above the ridge. The turbidity maxima of T1–T6, which have no 1st bin EI maxima in the western area, might represent the lower part of this "C" shape. If the lower part of the "C" exists below the AUV, it is very likely that the ADCP did not detect the signal.

A small amount of water might be advected eastward because the T9 turbidity maximum at the Archean site was found over the slope from the Snail site (Figs. 5 and 7b), however, this is not confirmed by the EI results in this study.

It is thought that scatterers of the ADCP beams were suspended particles in the water, small living animals such as zooplankton (Thomson *et al*., 1989), bubbles, and strong density stratifications. In a deep ocean such as the Southern Mariana Trough, and also in a hydrothermal field, it is expected that suspended particles and zooplankton are related to hydrothermal activity, if there is no other likely source. Besides, density stratification is quite weak in the deep sea. Therefore, it is inferred that EI is related to substances from hydrothermal plumes, rendering EI a very useful indicator for locating hydrothermal plumes. It is noted that microstructures of current velocity, temperature, and salinity also cause sound pulse reflection (Seim *et al*., 1995; Visbeck and Thurnherr, 2009), but these are likely to have a smaller effect.

Potential for application of EI anomaly to future plume detection

We summarize the analysis of turbidity and ADCP EI anomaly patterns for detecting hydrothermal plumes in Table 2, where an upward-looking ADCP on the AUV is used, as in this study. The ideal observation is Case 1, where both the turbidity and EI anomaly show a plume signal, as occurred over the Pika vent. In such a case, as a next step, the thickness of the EI maximum layer should be confirmed from the EI anomaly section in the upper layer of the AUV. Case 2 is an ordinal pattern when the ADCP is not used in observations. Case 3 is the most useful pattern for the ADCP, whereby the EI anomaly section indicates the plume thickness and the area without the turbidity sensor. This pattern was recognized on the deeper mound side of the Pika vent and the eastern part

of the Snail vent. If there is no signal from both of the sensors, as in Case 4, there might be EI maximum cores far above the AUV, which should be checked in the EI section.

In any case, if it is possible that a downward-looking ADCP can be attached to the AUV, the EI anomaly section in the lower layer should be obtained (Table 2). Simultaneously, side-scanning sonar might confirm the plume signal and its height just above vents; however, a non-buoyant plume has not been detected in previous studies (Kumagai *et al*., 2010; Asada *et al*., 2011). On the other hand, as this study suggests that the EI anomaly reflects not only buoyant plumes but non-buoyant plume advection as well, the ADCP observation method might be able to detect plumes in a larger range than side-scanning sonar without a continuous upward and downward movement of the AUV. This can result in highly effective AUVs and greater detection possibilities for future plume observations.

Conclusions

In this study, observations using a 600 kHz ADCP mounted on an AUV produced new 3D image views of EI anomalies (Figs. 4a and 4b). The characteristics and distribution of the high EI anomaly over well-known hydrothermal vents in the South Mariana Trough were described and examined. Multiple-range measurement with ADCPs, in combination with a single-point turbidity sensor, is effective for obtaining the thickness of plume layers, as the EI anomaly suggested a plume lower rim that was not detected by turbidity at the Snail vent. Over the vents, the high EI anomaly suggested a plume approximately 230 m thick at the Pika vent, 140 m thick at the Archean vent, and 160 m thick at the Snail vent, assuming that the EI anomaly reflects a hydrothermal signal. It is thought that these plumes are advected by a southward local mean current.

The results indicate that EI anomaly data can interpolate the sparse signals detected by a single-point turbidity sensor with a layer of more than 100 m. A larger number of EI maximum cores were obtained, and therefore, the plume distribution and advection/dispersal directions can be determined from these maxima in the same depth layer. Although side-scanning sonar only obtains buoyant plume signals below the AUV, it is likely that the upward-looking ADCP can describe non-buoyant plume signals in the upper layers. Combining this with a downward-looking ADCP would be an effective way to detect plumes in layers both above and below the AUV over a wide range, which is a promising application of the method for future plume surveys.

The general use of ADCPs in hydrothermal observations may also increase in terms of flux estimation of plumes, as the ADCP's primary function is measuring current velocity data. It might be possible for the ADCP to simultaneously calculate the density and dispersal speed of each EI maximum core in a plume during one dive, which would enable a new stage of more quantitative research on hydrothermal plumes.

Acknowledgments—We gratefully thank Takuroh Noguchi and Kei Okamura for the turbidity data, Miho Asada and Kyoko Okino for the topography data, and Satoshi Tsukioka for arranging the AUV raw datasets. Special appreciation goes to the anonymous reviewers who gave us highly suggestive comments.

References

Anderson, R. E., Torres Beltrán, M., Hallam, S. J. and Baross, J. A. (2013) Microbial community structure across fluid gradients in the Juan de Fuca Ridge hydrothermal system. *FEMS Microbiol. Ecol*. **83**, 324–339.

Asada, M., Nakamura, K., Mochizuki, N., Nogi, Y., Miyazaki, J., Kojima, S., Watanabe, H. and Okino, K. (2011) Volcanic and tectonic activities shown by a high-resolution acoustic survey, the case of the Southern Mariana Trough. *JGU Meeting 2011*, SIT002-06.

Asada, M., Yoshikawa, S., Mochizuki, N., Nogi, Y. and Okino, K. (2015) Examination of volcanic activity: AUV and submersible observations of fine-scale lava flow distributions along the Southern Mariana Trough spreading axis. *Subseafloor Biosphere Linked to Global Hydrothermal Systems; TAIGA Concept*, 469–478.

Baker, E. T., Massoth, G. J., Nakamura, K., Embley, R. W., De ronde, C. E. J. and Arculus, R. J. (2005) Hydrothermal activity on near-arc sections of back-arc ridges: Results from the Mariana Trough and Lau Basin. *Geochem. Geophys. Geosyst*. **6**(9), Q09001, doi:10.1029/2005GC000948.

Baker, E. T., Walker, S. L., Embley, R. W. and De ronde, C. E. J. (2012) High-resolution hydrothermal mapping of brothers caldera, Kermadec Arc. *Econ. Geol*. **107**, 1583–1593.

Beaulieu, S., Watanabe, H., Pradillon, F. and Kojima, S. (2011) International study of larval dispersal and population connectivity at hydrothermal vents in the U.S. Marianas Trench Marine National Monument. *InterRidge News* **20**, 50–54.

German, C. R., Richards, K. J., Rudnicki, M. D., Lam, M. M. and Charlou, J. L. (1998) Topographic control of a dispersing hydrothermal plume. *Earth Planet. Sci. Lett*. **156**, Express Letter, 267–273.

German, C. R., Yoerger, D. R., Jakuba, M., Shank, T. M., Langmuir, C. H. and Nakamura, K. (2008) Hydrothermal exploration with the Autonomous Benthic Explorer. *Deep-Sea Res. I* **55**, 203–219.

InterRidge Vents Database 2.2 (2015) Available at: http://www.interridge.org/irvents/ventfields

Ishibashi, J., Yamanaka, T., Kimura, H., Hirota, A., Toki, T., Tsunogai, U., Gamo, T., Utsumi, M., Roe, K., Miyabe, S. and Okamura, K. (2004) Geochemistry of hydrothermal fluids in South Mariana Backarc Spreading Center. *AGU Fall Meeting 2004*, V44A-05.

JAMSTEC (2009) *Yokosuka Cruise Report YK09-08 Mariana*

Trough Jun. 29, 2009–Jul. 17, 2009. Japan Agency for Marine-Earth Science and Technology (JAMSTEC).

Kakegawa, T., Utsumi, M. and Marumo, K. (2008) Geochemistry of sulfide chimneys and basement pillow lavas at the southern Mariana Trough (12.550N–12.580N). *Resour. Geol*. **58**, 249–266.

Komaki, K. and Ura, T. (2009) Observation of deep-currents in the Izena Caldron and the Beyonnaise Knoll Caldera by Towing an ADCP and DVL-mounted AUV. *ADCP's in Action 2009*, San Diego, U.S.A., abstract.

Komaki, K., Ura, T., Okamura, K., Koyama, H., Nagahashi, K., Shibasaki, H. and Hosoi, Y. (2010) Bottom-currents and high echo-intensity anomalies observed by ADCP-tows and AUV dives in the Izena Cauldron. *J. Japan Soc. Mar. Surv. Technol*. **22**(2), 23–37 (in Japanese with English abstract).

Kumagai, H., Tsukioka, S., Yamamoto, H., Tsuji, T., Shitashima, K., Asada, M., Yamamoto, F. and Kinoshita, M. (2010) Hydrothermal plumes imaged by high-resolution side-scan sonar on a crusing AUV, Urashima. *Geochem. Geophys. Geosyst*. **11**(12), Q12013, doi:10.1029/2010GC003337.

Nakamura, K., Toki, T., Mochizuki, N., Asada, M., Ishibashi, J., Nogi, Y., Yoshikawa, S., Miyazaki, J. and Okino, K. (2013) Discovery of a new hydrothermal vent based on an underwater, high-resolution geophysical survey. *Deep-Sea Res. I* **74**, 1–10.

Seim, H. E., Gregg, M. C. and Miyamoto, R. T. (1995) Acoustic backscatter from turbulent microstructure. *J. Atmos. Ocean Technol*. **12**, 367–380.

Takai, K., Komatsu, T., Inagaki, F. and Horikoshi, K. (2001) Distribution of archaea in a black smoker chimney structure. *Appl. Environ. Microbiol*. **67**, 3618–3629.

Thomson, R. E., Gordon, R. L. and Dymond, J. (1989) Acoustic doppler current profiler observations of a mid-ocean ridge hydrothermal plume. *J. Geophys. Res*. **94**(C4), 4709–4720.

Thomson, R. E., Burd, B. J., Dolling, A. G., Gordon, R. L. and Jamieson, G. S. (1992) The deep scattering layer associated with the Endeavour Ridge hydrothermal plume. *Deep-Sea Res*. **39**(1), 55–73.

Visbeck, M. and Thurnherr, A. M. (2009) High-resolution velocity and hydrographic observations of the Drygalski Trough gravity plume. *Deep-Sea Res. II* **56**, 835–842.

Wheat, C. G., Fryer, P., Hulme, S., Becker, N., Curtis, A. and Moyer, C. (2003) Hydrothermal venting in the southernmost portion of the Mariana backarc spreading center at 12°57′ N. *Eos Trans. AGU* **84**(46), Fall Meet. Suppl., abstract V32A-0920.

Yoshida-Takashima, Y., Nunoura, T., Kazama, H., Noguchi, T., Inoue, K., Akashi, H., Yamanaka, T., Toki, T., Yamamoto, M., Furushima, Y., Ueno, Y., Yamamoto, H. and Takai, K. (2012) Spatial distribution of viruses associated with planktonic and attached microbial communities in hydrothermal environments. *Appl. Environ. Microbiol*. **78**, 1311–1320.